Computational Fluid Dynamics Analysis of Shroud Design on Hemodynamic Performance and Blood Damage in a Centrifugal Blood Pump

Guangliang Pan[1], Yu Chang[1, *] and Mingrui Fu[1]

Abstract: Patients with extracorporeal membrane oxygenation still suffer from high rates of complication that linked to the flow field within the blood pump. So it is essential to optimise the geometry of the pump. The specification of shroud design is arguably the necessary design parameter in the centrifugal pump. However, the hemodynamic performances of the different shroud designs have not been studied extensively. In this study, ten different shroud designs were made and divided into two groups as the different covering locations (A: Covering the blade leading edge, B: Covering the blade trailing edge). In every group, six shroud designs with the covering proportions of 0,1/5,2/5,3/5,4/5,1 were made. Detailed computational fluid dynamics (CFD) analyses were performed to investigate their effects on hemodynamics and hydraulic performance at the constant flow condition (4000 rpm, 5 L/min). The percentage volumes of the scalar shear stress in specific threshold ($\tau<1$ Pa: Thrombosis, $\tau>9$ Pa: the destruction of von Willebrand factor, $\tau>50$ Pa: Platelet activation, $\tau>150$ Pa: Break of red blood) were used to compare the blood damage of the different shroud designs. Also, the modified index of hemolysis (MIH) were calculated based on a Eulerian approach for different pumps. CFD simulations predicted an increase in the pump head, hydraulic efficiency, a fraction of fluid volume with scalar shear stress values above a threshold (9 Pa, 50 Pa, 150 Pa) and MIH with increasing shroud covering proportions from 0 to 1 in the same covering location. Also, these above results were higher in group B than group A. This means that the risks of the hemolysis, thrombosis and bleeding increased as the rise of the covering proportion and they were higher in the pump whose shroud covers the blade trailing edge.

Keywords: Computational fluid dynamics (CFD), hemodynamics, centrifugal blood pump, shroud design, blood damage, thrombosis, hemolysis.

1 Introduction

Extracorporeal membrane oxygenation (ECMO) that based on the extracorporeal circulation system is a temporary artificial extracorporeal support of the respiratory system and cardiac system. It provides an effective treatment for many patients with life-threatening cardiopulmonary failure by using extracorporeal circulation technology.

---

[1] School of Life Science and BioEngineering, Beijing University of Technology, Beijing, 100124, China.

* Corresponding Author: Yu Chang. Email: changyu@bjut.edu.cn.

The report from the Extracorporeal Life Support Organization found that the use of ECMO had risen exponentially over the past years [ELSO (2017)]. However, the patients with ECMO still suffered from high rates of adverse events, such as bleeding, thrombosis and stroke. The blood pump as an essential component in ECMO provides the power for the blood, which means that most blood damage happens in the pump. So the optimisation of the flow geometry to maximise hydraulic performance while minimising shear-stress-induced hemolysis and thrombosis is very necessary for the pump design.

Nowadays many groups designed the pump geometry by using the automated optimisation frameworks [Wu, Shimmei, Tani et al. (2007); Yu, Janiga and Thevenin (2016)]; however, it was more important for the designer to gain insight into the impact of single design parameters. So far, many scholars had done a lot of researches on the hemodynamic performance of the leaves number, different blade shape and clearance gap size [Wannawat, Foojinphan, Khienwad et al. (2017); Wu, Paden, Borovetz et al. (2010); Kim, Diao, Ahn et al. (2009); Rezaienia, Paul, Avital et al. (2017); Graefe, Henseler and Steinseifer (2016); Chua, Yu, Leo et al. (1999)]. Some extensive experimental and analytical investigations had given the guidelines for shrouded and unshrouded industrial pump [Goto (1990); Engeda and Rautenberg (1987); Hirsch, Kang and Pointel (1996)]. But these studies just analysed the hydrodynamic characteristics; they did not consider the thrombogenicity and blood cell trauma which is the most important factors for blood pumps. The latter study [Wiegmann, Boës, Zélicourt et al. (2018)] focused on the hemodynamic performance and blood damage between the shrouded and unshrouded pump. However, it did not profoundly analyse the influence of the shroud designs with different covering proportions and locations.

Today computational fluid dynamics (CFD) analysis is widely used as a complementary tool for pump design in the early stages as it is an efficient and convenient way to analyse the flow patterns and pump efficiency. It had been used in the design and development of blood pumps since the 1990s [Sukumar, Athavale, Makhijani et al. (1996); Antaki, Ghattas, Burgreen et al. (1995)], along with other blood contacting devices [Wu, Taskin, Zhang et al. (2012); Fraser, Zhang, Taskin et al. (2010)]. Blood damage includes hemolysis, platelet activation, thrombosis and destruction of von Willebrand factor. Generally, hemolysis is evaluated by using the two approaches, Eulerian and Lagrangian. The damage index in the Eulerian approach is integrated over the entire computational flow domain whereas the integration is along the flow path lines in the Lagrangian approach. The Lagrangian approach encompasses the ability to calculate the shear stress history on the red blood cell, which enables the modelling of prior damage. The Eulerian method can give relative comparisons of hemolysis, and it would decrease calculation time and cost [Taskin, Fraser, Zhang et al. (2012)]. A fast three-dimensional numerical hemolysis approximation based on Eulerian method was made by Garon et al. [Garon and Farinas (2004)]. The modified index of hemolysis (MIH) was recommended as the most appropriate measurement in assessing the degree of hemolysis [ASTM.Designation: F 1841-97 (2013)]. And the computational pump design studies [Chang, Hur, Moshfeghi et al. (2015); Shou, Guo, Su et al. (2014)] reporting on hemocompatibility had typically focused on MIH based on Garon's model, and they found that it is an effective method to assess the hemolysis. So the fast numerical hemolysis approximation was used to compare the hemolysis of different pumps in this study. The platelet activation and slow

blood flow conditions are the main cause for the formation of thrombus. The von Willebrand factor(vWf) can be combined with collagen fibres and platelets. When the blood vessels ruptured, a large number of platelets were mediated by vWf, which adhere to collagen fibres and form clots to stop bleeding [Matsushita, Meyer and Sadler (2000); Sakariassen, Bolhuis and Sixma (1979)]. While the direct prediction of platelet activation and vWf break is currently not possible , therefore a quantitative comparison of mechanical blood damage parameters by calculating the fraction of fluid volume with the specific shear stress where platelet activation, vWf break, hemolysis, thrombosis happened had been served as alternatives to evaluate the hemocompatibility [Fraser, Zhang, Taskin et al. (2012)].

In this study, we provided a comprehensive investigation of the shroud designs with different covering proportions and locations given their hydrodynamic performance and hemodynamic characteristics. Our pump geometry was based on the ECMO centrifugal blood pump that our lab designed before. Computational fluid dynamics simulations were used to assess the velocity fields within the pump. Also, a further analysis had been done by the MIH and quantitative comparison of mechanical blood damage parameters by calculating the fraction of fluid volume with the specific shear stress where platelet activation, vWf break, hemolysis and thrombosis happened. In one word, these results shed light on the influence of shroud designs with different covering proportions and locations on shear stress distribution which is linked to the terms of blood damage.

2 Materials and methods

2.1 Pump geometrical models

The pump geometry of this study was motivated by a centrifugal blood pump developed by our group (see Fig. 1). This pump, having an 8-bladed impeller with a diameter of 50 mm, was designed using CFD-based design optimisation method for ECMO to deliver 5 L/min against 400 mmHg at 4000 rpm. Although the pump has not been used in the clinic, it is very close to the design of normal clinical blood pump through the test comparing the pump with the clinical blood pump (the Rotaflow pump, Maquet). To investigate the impact of shroud designs with different covering locations and covering proportions on the hemodynamic performance and blood damage, we devised ten different shroud designs. These ten pumps were designed with two design variations (covering location and covering proportion). For the covering location, two designs were selected, and they were divided into two groups (A: Cover the blade leading edge and let the blade trailing edge open, B: Cover the blade trailing edge and let the blade leading edge open). And the covering proportion (the length of the designed shroud/the length of the shroud in whole covering) was varied from 0 to 1; six different shrouds were made according to the covering proportion (0,1/5,2/5,3/5,4/5,1). Because the designs with the semi-open impeller (without shroud) and the closed impeller (in whole covering) were the same, they were named separately (C0: Semi-open impeller, C5: Closed impeller). There were ten shroud designs in all, and they were named respectively (A: C0, A1, A2, A3, A4, C5; B: C0, B1, B2, B3, B4, C5). The specific geometrical models of shrouds are shown in Fig. 2.
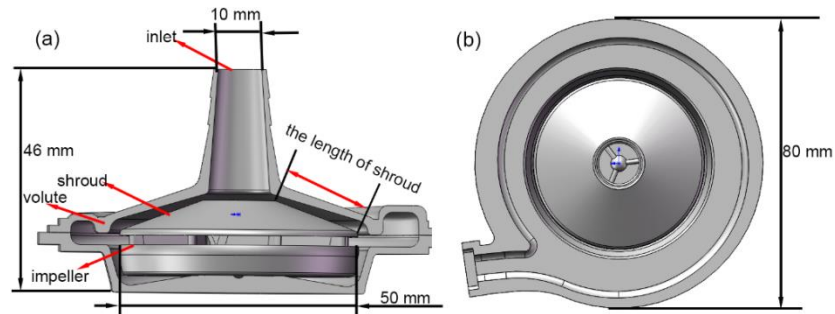
Figure 1: (a) Side view of the pump model of cut-open volute and impeller design as a basic model for the CFD simulations, (b) Top view of the pump model of the basic impeller and cut-open volute
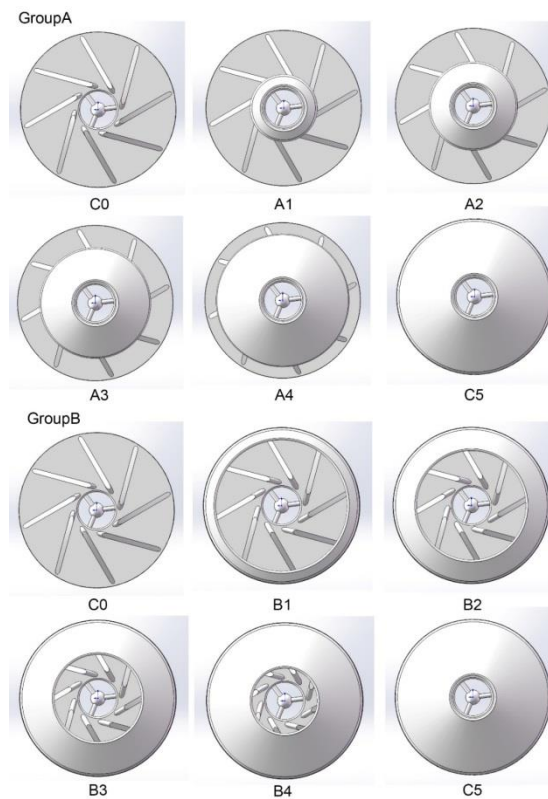
Figure 2: The specific geometrical models of shrouds

2.2 Computational fluid dynamics simulations

For this study, the computational meshes for the centrifugal blood pump were generated with the commercial software (Numeca_Hexpress, Belgium). They were composed of two blocks in total, incorporating a hexahedral structure with refinements near wall

regions and especially in blade regions. The grid sizes of the ten pump designs ranged between 9.1 million and 16.2 million. The numerical simulation of blood flow was calculated using the commercial CFD solver (Numeca_Fineopen, Belgium). For the centrifugal blood pump in this work, the representative Reynolds number was 97500 based on the impeller outlet diameter and the pump tip speed. So the shear stress transport (SST)-kω turbulence model was used in solving the turbulent Navier-Stokes equation. Blood was modelled as a Newtonian fluid with a viscosity of 3.5 mPa.s and a density of 1050 kg/m^3. It is well known that the blood is a non-Newtonian, but it is also a shear thinning fluid. Because the high shear rates found in the pump (>100 s^{-1}), it was treated as Newtonian. Operating condition plays one of the key roles in the hydraulic and hemodynamic performances of the blood pump, and then on the subsequent hemorheological results. Although the operating conditions might change according to individual difference, the ECMO pump needs to produce a flow rate 5 L/min against a pressure head of 400 mmHg to satisfy the clinical application [Chang, Hur, Moshfeghi et al. (2015)]. So the desired operating conditions were maintained constant for all designs performed in this study. The rotation of the impeller was implemented as a rigid body motion with a set speed of 4000 rpm. A uniform velocity distribution (1.2327 m/s) was applied as the inlet boundary condition while a pressure boundary condition was assumed for the outlet boundary. The simulations were carried out with a convergence criterion of 10^{-4} for the residual errors.

2.3 Scalar shear stress (SSS)

The scalar shear stress (τ) was calculated from the six viscous shear stress components (τ_{ij}) using the following equation according to the study of Bludszuweit [Bludszuweit (1995)].

$$\tau = \left[\frac{1}{6}\Sigma(\tau_{ii} - \tau_{jj})(\tau_{ii} - \tau_{jj}) + \Sigma(\tau_{ij}\tau_{ij})\right]^{1/2} \tag{1}$$

where the components of the scalar shear stress tensor were computed from the viscous stress only based on the blood damage models available in the literature [Johnson and Meller (1973)].

The fractions of the fluid volume whose scalar shear stress above the threshold suspected for vWf cleavage(τ>9 Pa), platelet activation (τ>50 Pa) and hemolysis(τ>150 Pa) of the total volume were calculated to assess the risk of bleeding, thrombosis and hemolysis [Fraser, Zhang, Taskin et al. (2012)]. Shear stresses of less than 1pa had been related to thrombosis, therefore the volume percentage (τ<1 Pa) was calculated to evaluate the thrombosis [Hochareon, Manning, Fontaine et al. (2004)].

2.4 MIH

The rate of hemolysis of the ten centrifugal blood pumps was evaluated by computing the modified index of hemolysis (MIH) [ASTM. Designation: F 1841-97. (2013)] using a Eulerian scalar transport approach. To predict the MIH for the different pumps, Garon and Farinas [Garon and Farinas (2004)] proposed a new fast numerical hemolysis approximation based on the power law-based model developed by Giersiepen et al. [Gieriepen, Wurzinger, Opitz et al. (1990)]. Equations give formulas 2-6.

$$D = 3.62 \times 10^{-7} \tau^{2.416} t^{0.785} \tag{2}$$

$$D_I = D^{1/0.785} = (3.62 \times 10^{-7})^{1/0.785} \tau^{2.416/0.785} t \tag{3}$$

$$\sigma = \frac{d}{d_t} D_I = (3.62 \times 10^{-7})^{1/0.785} \tau^{2.416/0.785} \tag{4}$$

$$\overline{D_I} = \frac{1}{Q} \int \sigma \, dV \tag{5}$$

$$D = \left(\overline{D_I}\right)^{0.785} \tag{6}$$

$$MIH = D \times 10^6 \tag{7}$$

Where D_I is the linear damage, σ is source related to the scalar shear stress τ, Q is the flow rate, $\overline{D_I}$ is the average linear damage.

The Eq. (4) represents the rate of hemolysis production per unit of time, and shear stress (τ) in this equation is a function of the velocity field obtained from the numerical simulations of blood flow. Equations from 4-7 constitute the hemolysis prediction model. In contrary to the approach using the calculation of the damage along with some particle pathlines, this model integrates over the entire computational domain to take in the count all areas contributing to the hemolysis. It can give a global index to evaluate the hemolysis degree, and the procedure is efficient and cost-effective.

3 Results

3.1 Pump head and hydraulic efficiency

The influence of the ten blood pumps with different shroud designs on the pump head and hydraulic efficiency is shown in Fig. 3.
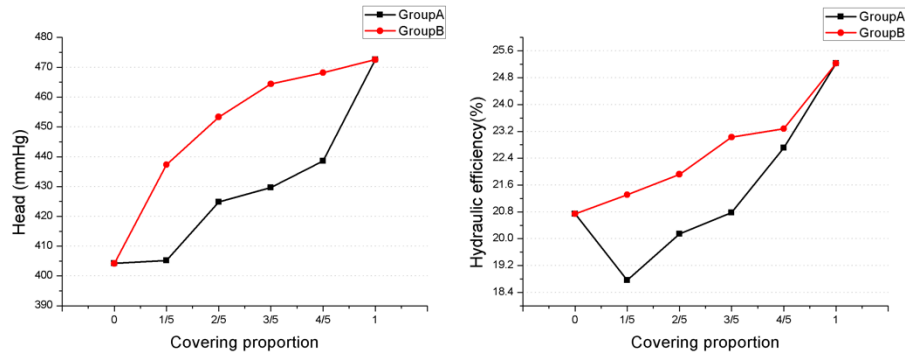
Figure 3: Computed pump head and hydraulic efficiency plotted for variation of the shroud design

The pump head ranged between 404.2 mmHg and 472.58 mmHg, and the hydraulic efficiency was between 18.76% and 25.23% at the flow condition (flow rate=5 L/min, impeller speed=4000 rpm). In group A, the pump head had a monotone increase from 404.2 mmHg to 472.58 mmHg (+16%) as the covering proportion of the shroud rises from 0 to 1. The tendency was the same in the group B, while the pump head in group B was higher than that in group A in the same covering proportion. Although the efficiency

decreased from 20.74 to 18.76% as the covering proportion increased from 0-1/5 in group A, it steadily increased from 18.76%-25.23% with the increase of the proportion (1/5-1). In group B, the efficiency gradually increased from 20.74% -25.23% with the rise of the covering proportion and the efficiency was larger than group A in the same covering proportion.

3.2 Velocity fields

The velocity fields for the ten centrifugal blood pumps with different shroud designs are shown in Fig. 4. Summaries of these velocity fields are given below.
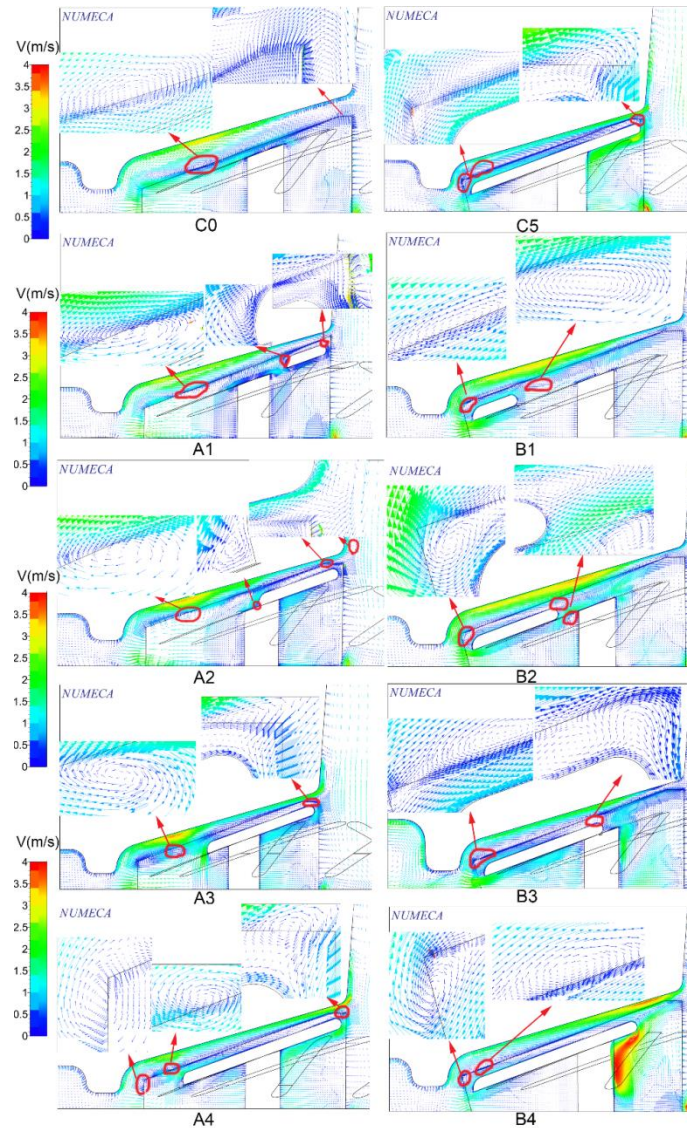
Figure 4: Velocity fields around the shroud in the ten pumps with different shroud designs

The regions marked with red circles were the recirculation zones near the shroud, and the arrows pointed the amplifying picture of the recirculation zones. There was only one recirculation zone between the impeller and the housing in the model C0 designed with an unshroud impeller. But if the pump was designed with a shroud in the impeller, more recirculation zones occurred between the impeller and housing. And the recirculation zones happened in the inlet and outlet of the shroud.

3.3 Scalar shear stress

The distribution of the scalar shear stress in the block of the impeller is shown in Fig. 5. It was easy to find that the high shear stress happened on the leading and trailing edge of the blades. Also, the scalar shear stress was becoming higher as the increase of radial distance. In this study, four different thresholds ($\tau < 1$ Pa, $\tau > 9$ Pa, $\tau > 50$ Pa, $\tau > 150$ Pa) of the scalar shear stress were used to evaluate the blood damage. The fractions of fluid volume with scalar shear stress in these thresholds of the total fluid volume are shown in Fig. 6.
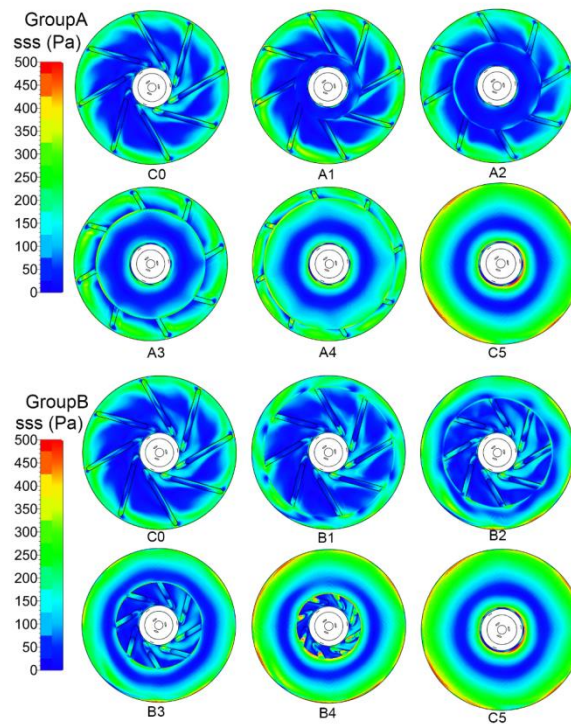
Figure 5: Distribution of scalar shear stress on the block of the impeller
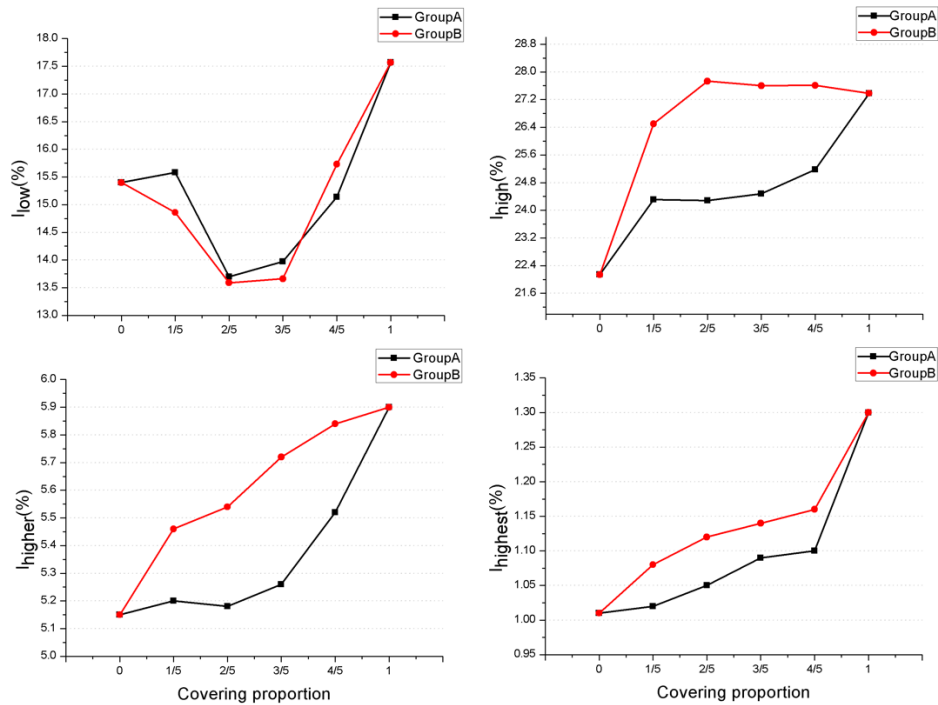
Figure 6: Fraction of fluid volume with scalar shear stress in specific thresholds (low sss volume=volume with sss<1 Pa, high sss volume=volume with sss>9 Pa, higher sss volume=volume with sss>50 Pa, highest sss volume=volume with sss>150 Pa) of the total fluid volume

The volume in the scalar shear stress range (τ<1 Pa) based on the study of Hochareon et al. [Hochareon, Manning, Fontaine et al. (2004)] was calculated, and it was called low sss volume in this study. The fractions of low sss volume of the total fluid volume (I_{low}) were calculated, and the results were shown in Fig. 6. In group A, I_{low} did not have a monotonous trend with the increase of covering proportion, and it was in the range of 13.7(A2)-17.57%(C5). The trend of I_{low} in group B was similar to group A, and it was in the range of 13.59(B2)-17.57%(C5).

For this study, a threshold of 9 Pa was used as an indicator of the potential to break the vWf, and it was called high sss volume [Di and De (2010)]. The fraction of high sss volume of the total fluid volume (I_{high}) increased steadily from 22.14%(C0) to 27.38%(C5) when the covering proportion increased in group A. In group B, the values of I_{high} increased from 22.14%-27.73% when the covering proportion increased from 0 to 2/5. However, as the proportion increased from 2/5-1, I_{high} remained relatively constant at 27.5%. Also, it was obvious that the I_{high} in group B was higher than which in group A in the same covering proportion.

Regions with sss greater than 50 Pa were called higher sss regions for a threshold of 50 Pa was used as an indicator of potential platelet activation [Hellums (1994)]. The fraction of higher sss volume of the total fluid volume (I_{higher}) was calculated to assess the potential possibility of thrombosis. The trend of the values of I_{higher} in group A and group

B was the same; it rose from 5.15%-5.9% as the covering proportion increasing. However, the values of I_{higher} in group B was larger in the same covering proportion.

Shear stress above 150 Pa had been linked with hemolysis [Alemu and Bluestein (2007)], and thus the regions with an sss above 150 Pa were termed highest sss. The fraction of highest sss volume of the total fluid volume ($I_{highest}$) steadily increased with increasing covering proportion in both group A and group B. Additionally, $I_{highest}$ in group B was higher in the same covering proportion.

The areas of shroud exposed to the highest scalar shear stress ($\tau > 150$ Pa) mostly happened near the blade trailing edge and on the inlet and the outlet of the shroud (see Fig. 7). As the rise of the covering proportion of shroud in both Group A and Group B, the areas of highest scalar shear stress were not only located in the increased shroud area, but also the areas where used to be lower than 150 Pa were exposed to the highest scalar shear stress. Also, the areas of highest scalar shear stress in Group B was higher than which in group A.
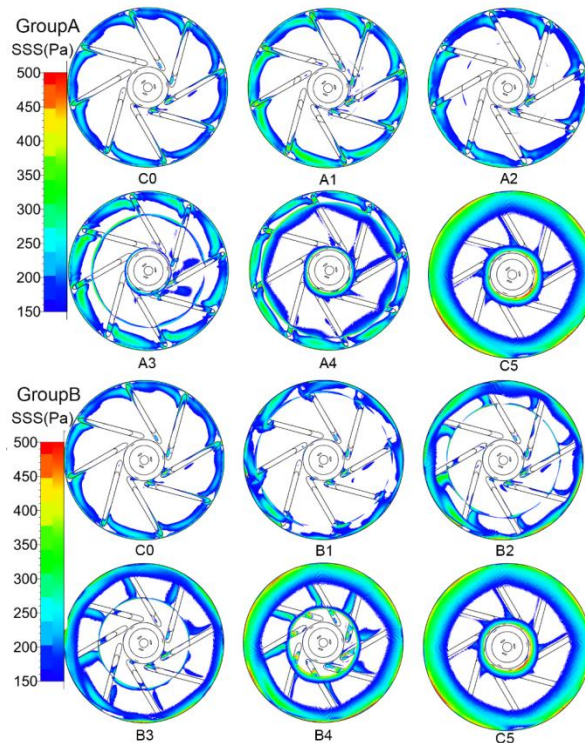
Figure 7: Areas of highest scalar shear stress ($\tau > 150$ Pa) in the impeller

3.4 MIH

The fast three-dimensional numerical hemolysis approximation currently available in the literature had been found to accurately predict relative comparisons of hemolysis in centrifugal blood pumps with different shroud designs. As was mentioned before, the modified index of hemolysis (MIH) was calculated to evaluate the hemolysis in the ten

models (see Fig. 8). Increasing the covering proportion from 0-1, MIH increased by 32% from 1350-1810 in group A. MIH in group B also had a similar tendency, but it was higher than that in group A in the same covering proportion.
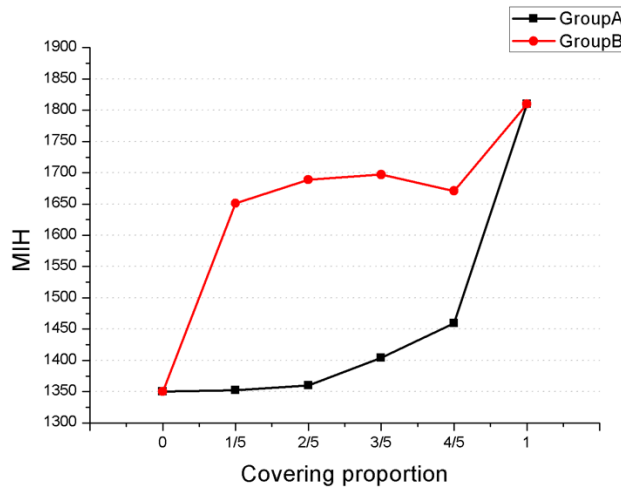
Figure 8: Computation of the MIH for the ten centrifugal pumps

4 Discussion

In this study, the CFD simulations were performed to gain a better understanding of the influence of different shroud designs on hemodynamic performance and blood damage. Flow fields in the centrifugal pumps with ten different shroud designs were calculated, using CFD at operating condition (4000 rpm, 5 L/min) and multiple metrics of hydraulic performance were analysed. Also, a fast three-dimensional numerical hemolysis approximation was used, and the modified index of hemolysis (MIH) was calculated to compare hemolysis in the different pumps.

CFD simulations reported here showed that the increasing shroud covering proportion caused a rise in pump head and hydraulic efficiency (Fig. 3), which is consistent with the previous numerical study of the hydraulic performance between the semi-open impeller and the closed shroud [Wiegmann, Boës, Zélicourt et al. (2018)]. This is possible because the blade tip clearance may account for over one-third of the hydraulic efficiency of a pump [Dey and Camci (2000)] and the shroud design decreases the blade tip clearance between the impeller and the stationary housing. Additionally, the pump head and hydraulic efficiency of the pumps whose shrouds cover the blade trailing edge were higher than the designs whose shrouds cover the blade leading edge. It could also be partly due to the velocity in the blade trailing edge is higher; hence the shroud covering the blade trailing edge decreased more leakage flow than which covering the blade leading edge.

There was a nonlinear tendency in volumes exposed to low sss as the shroud covering proportion increased, while the percentage volumes experiencing high (>9 Pa), higher (>50 Pa), highest (>150 Pa) sss had an increasing trend with the rise of the shroud covering proportion (Fig. 6). In contrast, L.Wiegmann et al. [Wiegmann, Boës, Zélicourt et al.

(2018)] reported that compared to the semi-open design, the closed shroud design reduced the number of the particles exposed to high shear stress (>50 Pa and >150 Pa). Different to our study, they studied the effect of the shroud design prescribing a constant static pressure head of 100 mmHg. Also, as compared to the shroud covering the blade trailing edge, the shroud covering the blade leading edge decreased the zones that exposed to high sss, higher sss and highest sss. This is possible because that the velocity in the blade trailing edge is higher than which in the blade leading edge; hence the shroud covering the blade trailing edge cause higher sss.

The calculation of MIH revealed a positive correlation between hemolysis and covering proportion: larger covering proportion caused the rise of the erythrocytes trauma. Hence the semi-open impeller is the best design for causing lest damage in erythrocytes (Fig. 8). Similar trends had been observed previously in the numerical study of hemolysis in the shroud designs with the semi-open impeller and a closed shroud impeller [Wiegmann, Boës, Zélicourt et al. (2018)].

5 Conclusions

The detailed flow patterns presented in this study revealed some interesting fluid dynamic features associated with the covering proportion and location of the shroud. CFD simulations of a centrifugal blood pump with 50 mm impeller predicted a rise in the percentage volumes experiencing high (>9 Pa), higher (>50 Pa) and highest (>150 Pa) scalar shear stress and modified index of hemolysis (MIH) with increasing covering proportion of shroud in the same covering location. And the results of above were higher in group B than group A. These revealed that the increase of the proportion of shroud would cause more risk of the destruction of vWf, the activation of platelet and the damage of red blood. In addition to this, the velocity fields in the ten pumps showed that the impeller with shroud design would cause more recirculation zones which happened in the inlet and outlet of the shroud than the impeller with an unshroud design. In conclusion, the shroud with the lower covering proportion had a less damage in blood, and the shroud covering the blade trailing edge caused more blood damage than the blade leading edge.

References

Alemu, Y.; Bluestein, D. (2007): Flow-induced platelet activation and damage accumulation in a mechanical heart valve: Numerical studies. *Artificial Organs*, vol. 31, no. 9, pp. 677-688.

Antaki, J. F.; Ghattas, O.; Burgreen, G. W.; He, B. (1995): Computational flow optimization of rotary blood pump components. *Artificial Organs*, vol. 19, no. 7, pp. 608-615.

ASTM Designation (F 1841-97) (2013): Standard practice for assessment of hemolysis

in continuous flow blood pumps. *Annual Book of ASTM Standards*.

Bludszuweit, C. (1995): Model for a general mechanical blood damage prediction. *Artificial Organs*, vol. 19, no. 7, pp. 583.

Chang, M.; Hur, N.; Moshfeghi, M.; Kang, S.; Kim, W. et al. (2015): A numerical study on mechanical performance and hemolysis for different types of centrifugal blood pumps. *ASME 2015 International Mechanical Engineering Congress and Exposition*.

Chua, L. P.; Yu, S. C. M.; Leo H. L.; Chan, W. K. (1999): Comparison of flow characteristics of enlarged blood pump models with different impeller design. *International Communications in Heat & Mass Transfer*, vol. 26, no. 3, pp. 369-378.

Dey, D.; Camci, C. (2000): Development of tip clearance flow downstream of a rotor blade with coolant injection from a tip trench. *Proceedings of the 8th International Symposium on Transport Phenomena and Dynamics of Rotating Machinery*, pp. 572-579.

Di, S. E.; De, C. R. (2010): The effect of shear stress on protein conformation: Physical forces operating on biochemical systems: The case of von Willebrand factor. *Biophysical Chemistry*, vol. 153, no. 1, pp. 1-8.

Engeda, A.; Rautenberg, M. (1987): Comparisons of the relative effect of tip clearance on centrifugal impellers. *Journal of Turbomachinery*, vol. 109, no. 4, pp. 545-549.

Extracorporeal Life Support Organization. (2017): 2017 annual report: Extracorporeal life support organization. https://www.elso.org/Home.aspx

Fraser, K. H.; Zhang, T.; Taskin, M. E.; Griffith, B. P.; Wu, Z. J. (2010): Computational fluid dynamics analysis of thrombosis potential in left ventricular assist device drainage cannulae. *Asaio Journal*, vol. 56, no. 3, pp. 157.

Fraser, K. H.; Zhang, T.; Taskin, M. E.; Griffith, B. P.; Wu, Z. J. (2012): A quantitative comparison of mechanical blood damage parameters in rotary ventricular assist devices: Shear stress, exposure time and hemolysis index. *Journal Biomechanical Engineering*, vol. 134, no. 8, pp. 1002.

Garon, A.; Farinas, M. (2004): Fast three-dimensional numerical hemolysis approximation. *Artificial Organs*, vol. 28, no. 11, pp. 1016-1025.

Giersiepen, M.; Wurzinger, L. J.; Opitz, R.; Reul, H. (1990): Estimation of shear stress-related blood damage in heart valve prostheses-in vitro comparison of 25 aortic valves. *International Journal of Artificial Organs*, vol. 13, no. 5, pp. 300.

Goto, A. (1990): Study of internal flows in a mixed-flow pump impeller at various tip clearances using three-dimensional viscous flow computations. *Journal of Turbomachinery*, vol. 114, no. 2, pp. 373-382.

Graefe, R.; Henseler, A.; Steinseifer, U. (2016): Multivariate assessment of the effect of pump design and pump gap design parameters on blood trauma. *Artificial Organs*, vol. 40, no. 6, pp. 568-576.

Hellums, J. D. (1994): 1993 Whitaker Lecture: Biorheology in thrombosis research. *Annals of Biomedical Engineering*, vol. 22, no. 5, pp. 445-455.

Hirsch, C.; Kang, S.; Pointel, G. A. (1996): Numerically supported investigation of the 3-D flow in centrifugal impellers. Part II: Secondary flow structure. *American Society of*

Mechanical Engineers.

Hochareon, P.; Manning, K. B.; Fontaine, A. A.; Tarbell, J. M.; Deutsch, S. (2004): Correlation of *in vivo* clot deposition with the flow characteristics in the 50 cc penn state artificial heart: A preliminary study. *Asaio Journal*, vol. 50, no. 6, pp. 537-542.

Johnson, W. H.; Meller, P. B. (1973): *Engineering Plasticity*. Van Nostrand Reinhold Co., USA.

Kim, N. J.; Diao, C.; Ahn, K. H.; Lee, S. J.; Kameneva, M. V. et al. (2009): Parametric study of blade tip clearance, flow rate, and impeller speed on blood damage in rotary blood pump. *Artificial Organs*, vol. 33, no. 6, pp. 468-474.

Matsushita, T.; Meyer, D.; Sadler, J. E. (2000): Localization of von willebrand factor-binding sites for platelet glycoprotein Ib and botrocetin by charged-to-alanine scanning mutagenesis. *Journal of Biological Chemistry*, vol. 275, no. 15, pp. 11044-11049.

Rezaienia, M. A.; Paul, G.; Avital, E.; Rothman, M. T.; Korakianitis, T. (2017): Computational parametric study of the axial and radial clearances in a centrifugal rotary blood pump. *Asaio Journal*.

Sakariassen, K. S.; Bolhuis, P. A.; Sixma, J. J. (1979): Human blood platelet adhesion to artery subendothelium is mediated by factor VIII-Von Willebrand factor bound to the subendothelium. *Nature*, vol. 279, no. 5714, pp. 636-638.

Shou, C.; Guo, Y.; Su, L.; Li, Y. (2014): Numerical assessment of impeller features of centrifugal blood pump based on fast hemolysis approximation model. *Journal of Biomedical Engineering*, vol. 31, no. 6, pp. 1260-1264.

Sukumar, R.; Athavale, M. M.; Makhijani, V. B.; Przekwas, A. J. (1996): Application of computational fluid dynamics techniques to blood pumps. *Artificial Organs*, vol. 20, no. 5, pp. 529-533.

Taskin, M. E.; Fraser, K. H.; Zhang, T.; Wu, C.; Griffith, B. P. et al. (2012): Evaluation of Eulerian and Lagrangian models for hemolysis estimation. *Asaio Journal*, vol. 58, no. 4, pp. 363-372.

Wannawat, P.; Foojinphan, N.; Khienwad, T.; Naiyanetr, P. (2017): The study of various impeller design for centrifugal blood pump using computer method. *Iasted International Conference on Biomedical Engineering*.

Wiegmann, L.; Boës, S.; Zélicourt, D. D.; Thamsen, B.; Daners, M. S. et al. (2018): Blood pump design variations and their influence on hydraulic performance and indicators of hemocompatibility. *Annals of Biomedical Engineering*, vol. 46, no. 3, pp. 417-428.

Wu, J.; Paden, B. E.; Borovetz, H. S.; Antaki, J. F. (2010): Computational fluid dynamics analysis of blade tip clearances on hemodynamic performance and blood damage in a centrifugal ventricular assist device. *Artificial Organs*, vol. 34, no. 5, pp. 402-411.

Wu, J.; Shimmei, K.; Tani, K.; Niikura, K.; Sato, J. (2007): CFD-based design optimization for hydro turbines. *Journal of Fluids Engineering*, vol. 129, no. 2, pp. 159-168.

Wu, Z. J.; Taskin, M. E.; Zhang, T.; Fraser, K. H.; Griffith, B. P. (2012): Computational

model-based design of a wearable artificial pump-lung for cardiopulmonary/respiratory support. *Artificial Organs*, vol. 36, no. 4, pp. 387-399.

Yu, H.; Janiga, G.; Thévenin, D. (2016): Computational fluid dynamics-based design optimization method for archimedes screw blood pumps. *Artificial Organs*, vol. 40, no. 4, pp. 341-352.